Scholars Research Library

Der Pharma Chemica, 2014, 6(5):383-406
(http://derpharmachemica.com/archive.html)

ISSN 0975-413X
CODEN (USA): PCHHAX

A DFT Study of the Relationships between the Electronic Structures of a series of 2,4,5-Trisubstituted Pyrimidines and their Inhibition of four Cyclin-dependent Kinases and their Anti-Proliferative Action against HCT-116 and MCF-7 Cell Lines.

Javier Valdebenito-Gamboa and Juan S. Gómez-Jeria*

Quantum Pharmacology Unit, Department of Chemistry, Faculty of Sciences, University of Chile, Las Palmeras 3425, Santiago 7800003, Chile

---

ABSTRACT

We present a study of the relationships between the electronic structures of a series of 2,4,5-trisubstituted pyrimidines and their inhibition of four cyclin-dependent kinases. Also we present a similar analysis concerning their anti-proliferative action against the MCF-7 and HCT-116 cell lines. The electronic structure of all the molecules was obtained using Density Functional Theory at the B3LYP/6-31g(d,p) level with full geometry optimization. We found statistically significant relationships between the variation of several local atomic reactivity indices and the variation of biological activity for all cases analyzed. The corresponding partial pharmacophores are proposed. In the case of the anti-proliferative action against MCF-7 and HCT-116 cell lines, the results strongly suggest that the site of action of all the molecules studied is located somewhere in the cell replication system. The possible relationships between the molecular electrostatic potential structure and the partial pharmacophores are discussed for some examples.

Keywords: Pyrimidines, cyclin-dependent kinases, HCT-116, MCF-7, CDK, QSAR, antitumor action, DFT, electronic structure.

INTRODUCTION

Cyclin-dependent kinases (CDKs) are the catalytic subunits of a family of mammalian heterodimeric serine/threonine kinases. The cell cycle sequence is controlled by a arrangement of CDKs, which control the progression along four consecutive phases: the gap phase G1 (the phase during which the cell grows and carries out large amounts of protein synthesis), the S phase of DNA replication (the phase during which the genomic DNA is replicated), the gap phase G2 and the M or mitotic phase [1-18] (and references therein). CDKs are activated by the binding of a regulatory subunit, for the most part generally, but not solely, a cyclin. CDKs are also regulated by interactions with inhibitory proteins, by activating or inhibitory phosphorylations, by transient intracellular translocations and by the periodic proteolytic degradation of their activating cyclin partner. It was noted that cancer cells frequently rely on increased CDK signaling which manifests, for example, in an augmented rate of cell cycling and cellular hyperproliferation [7, 19-35] (and references therein). Over the past twenty years CDK4 and CDK6 have been identified as the most important oncogenic drivers among cell cycle kinases. Both these kinases are rendered hyperactive throughout a wide diversity of mechanisms in human cancer, including frequent amplification or mutation of their genes. Many molecular systems have been synthesized and tested for CDK inhibition and potential antitumor activity [36-75]. Recently, Wang et al. synthesized a series of 2,4,5-trisubstituted pyrimidines and tested them for CDK inhibition and anti-proliferative activities [40]. In this paper, and with the aim of providing more detailed and physically-based information, we present the results of a quantum-chemical analysis relating the

electronic structures of the above mentioned molecules with their CDK inhibitory potencies and anti-proliferative activities.

MATERIALS AND METHODS

METHODS, MODELS AND CALCULATIONS

The model

Considering that the model employed here has been the subject of discussion in several papers and has been widely applied, we present here the final resulting equation [76-103]. The logarithm of any biological activity (BA) can be written as:

$$\log(BA)=cte+\sum_i\left[e_iQ_i+f_iS_i^E+d_iS_i^N\right]+$$
$$+\sum_i\sum_m\left[h_i(m)F_i(m)+x_i(m)S_i^E(m)\right]+\sum_i\sum_{m'}\left[r_i(m')F_i(m')+t_i(m')S_i^N(m')\right]+$$
$$+\sum_i\left[g_i\mu_i+k_i\eta_i+o_i\omega_i+z_is_i+w_iQ_i^{max}\right]+\sum_{B=1}^{W}O_B \qquad (1)$$

where Q_i is the net charge of atom *i*, S_i^E and S_i^N are the total atomic electrophilic and nucleophilic superdelocalizabilities of atom i, $F_{i,m}$ is the Fukui index of the occupied [empty] molecular orbitals (MO) m [m'] located on atom i. $S_i^E(m)$ is the local atomic electrophilic superdelocalizability of MO m on atom i, etc. The total atomic electrophilic superdelocalizability of atom i corresponds to the sum over occupied MOs of all the $S_i^E(m)$'s and the total atomic nucleophilic superdelocalizability of atom i is the sum over empty the MOs of all $S_i^N(m')$'s [104]. The last bracket of Eq. 1 contains the local atomic electronic chemical potential of atom i, the local atomic hardness of atom i, the local atomic electrophilicity of atom i, the local atomic softness of atom i and the maximal amount of electronic charge that atom i may receive [105, 106]. For example, the local atomic electronic chemical potential of atom i, μ_i, is defined as:

$$\mu_i=\frac{E_{oc}^*-E_{em}^*}{2} \qquad (2)$$

where E_{oc}^* is the highest occupied MO located on atom with a non-zero Fukui index and E_{em}^* is the lowest vacant MO located on atom i with a non-zero Fukui index. The total local atomic hardness of atom i, η_i, is defined as:

$$\eta_i=E_{em}^*-E_{oc}^* \qquad (3)$$

η_i corresponds to the local $HOMO_i$*-$LUMO_i$* gap. The total local atomic softness of atom i, s_i, is defined as the inverse of the local atomic hardness. O_B is the orientational parameter of substituent B and it has been interpreted as the influence of the substituent on the fraction of molecules attaining the proper orientation to interact with a given site.

Selection of molecules and experimental data

The selected molecules are shown in Fig. 1 and Table 1 [40].

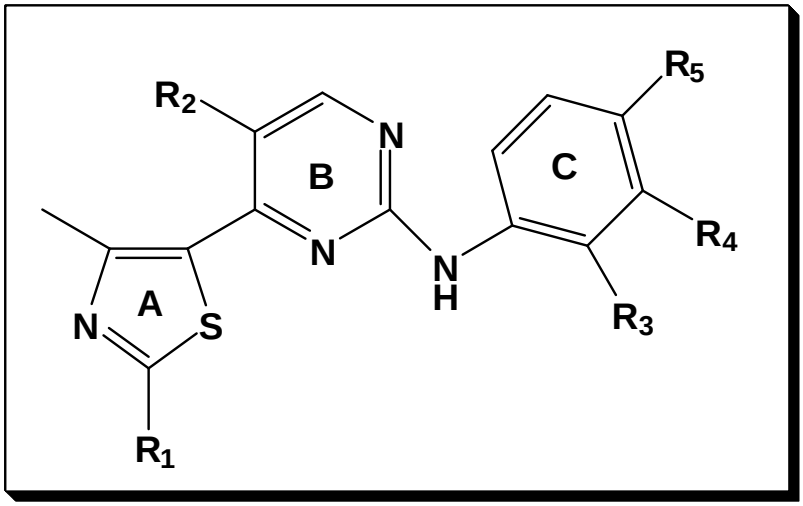

Figure 1. General formula of the 2,4,5-trisubstituted pyrimidines.

Table 1. Structures of the 2,4,5-trisubstituted pyrimidines.

Mol.	R_1	R_2	R_3	R_4	R_5
1	NH_2	F	H	$-SO_2NH_2$	H
2	NH_2	F	H	4-acetylpiperazin-1-yl	H
3	NHMe	F	H	-4-acetylpiperazin-1-yl	H
4	NH_2	F	H	-4-acetylpiperazin-1-yl	H
5	NHMe	CN	H	$-SO_2Me$	H
6	NHMe	CN	H	$-SO_2NH(CH_2)_2Me$	H
7	NHMe	F	H	$-SO_2NH(CH_2)_2Me$	H
8	NHMe	CN	H	$-SO_2$-morpholin-4-yl	H
9	NHMe	H	H	$-SO_2$-morpholin-4yl	Me
10	NHMe	F	H	$-SO_2$-morpholin-4-yl	Me
11	NHMe	CN	H	$-SO_2$-4-methylpiperazin-1-yl	H
12	NHMe	H	H	-CO-morpholin-4-yl	H
13	NHMe	CN	H	-CO-morpholin-4-yl	H
14	NHMe	CN	H	-CO-4-acetylpiperazin-1-yl	H
15	NHMe	CN	H	-CO-4-methylpiperazin-1-yl	H
16	NHMe	CN	Cl	-CO-4-methylpiperazin-1-yl	H
17	NHMe	F	H	-CO-N-(1-methylpiperidin-4-yl)	H
18	NHMe	CN	H	H	p-CO-N-(1-methylpiperidin-4-yl)
19	NHMe	CN	H	-CO-N-(1-methylpiperidin-4-yl)	H

The reported experimental data employed in this study are shown in Table 2. They are the apparent inhibition constants (K_i) of CDK9T1, CDK1B, CDK2A and CDK7H, and the concentrations required to inhibit 50% of cell growth (GI_{50}) of HCT-116 and MCF-7 cell lines [40].

Calculations

The electronic structure of the molecules was obtained with Density Functional Theory at the B3LYP/6-31g(d,p) level using the Gaussian suite of programs [107]. After full geometry optimization and single point calculations, the values of the LARIs were calculated with D-CENT-QSAR [108]. Negative electron populations or MO populations greater than 2 arising from Mulliken Population Analysis were corrected as usual [109]. Orientational parameters were calculated as usual [110]. We used Linear Multiple Regression Analysis (LMRA) to find which atoms are involved in the variation of the biological activity. We worked with the hypothesis that there is a set of atoms common to all the molecules (the common skeleton), encoding the variation of the biological activity throughout the group of molecules. It is the variation of the values of one or more local atomic reactivity indices of the atoms of the common skeleton that accounts for the variation of the biological activities. The substituents modify the electronic structure of the common skeleton and direct the precise orientation of the common skeleton with its partner through the orientational parameters. For each LMRA, we built a matrix containing the logarithm of the dependent variable,

the local atomic reactivity indices of the atoms constituting the common skeleton and the orientational parameters of substituents R_1 to R_5. Statistica software was used for LMRA [111]. The common skeleton numbering is shown in Fig. 2.

Table 2. Biological activities of the 2,4,5-trisubstituted pyrimidines.

Mol.	log(K_i) CDK9T1	log(K_i) CDK1B	log(K_i) CDK2A	log(K_i) CDK7H	log(GI_{50}) HCT-116	log(GI_{50}) MCF-7
1	0.48	0.85	0.48	2.40	-1.30	-0.39
2	1.04	1.61	1.89	3.16	-0.77	-0.38
3	0.85	1.51	1.62	2.73	-0.29	-0.21
4	1.04	1.81	1.83	2.68	-1.05	-1.05
5	0.70	1.28	1.63	2.04	-0.70	-0.37
6	1.20	1.53	1.34	2.26	-0.72	-0.59
7	0.48	1.00	0.30	1.48	-0.52	-0.14
8	1.15	1.86	1.74	2.95	-0.52	-0.09
9	1.43	2.57	2.47	2.18	-0.03	0.21
10	1.04	2.00	2.11	2.12	-0.15	0.18
11	1.54	2.76	2.77	1.38	-0.21	0.06
12	1.98	2.42	2.69	2.59	-0.28	-0.26
13	1.63	2.31	2.30	3.27	-0.23	-0.09
14	1.23	2.22	2.13	2.74	0.77	0.70
15	1.28	2.50	2.21	2.92	-0.14	0.14
16	2.85	NA	NA	NA	0.17	0.29
17	1.56	1.81	2.36	2.73	-0.33	-0.03
18	0.90	1.63	1.51	2.48	-0.74	-0.29
19	1.15	2.42	2.50	2.21	-0.10	-0.19

NA. Not available.

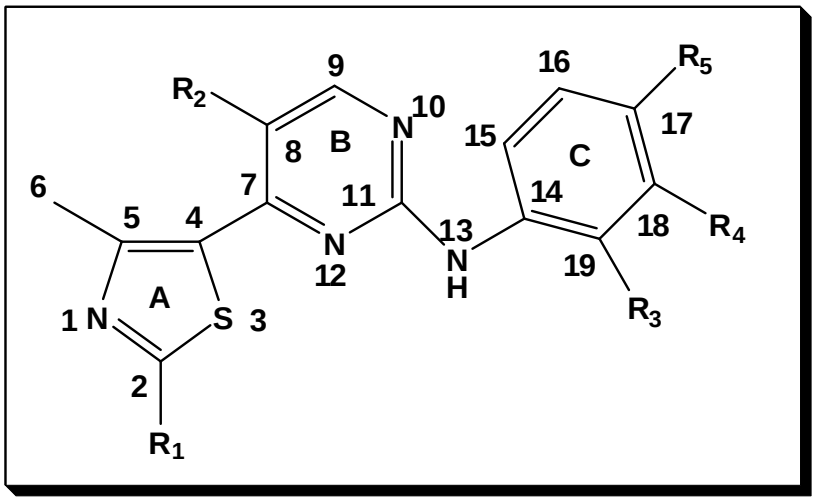

Figure 2. Common skeleton numbering of the 2,4,5-trisubstituted pyrimidines.

The molecular electrostatic potential (MEP) maps were obtained with Molekel and GaussView programs [112, 113]. The latter program was also used for the depiction of molecular orbitals.

RESULTS

Table 3 shows the correlation among the different CDK inhibition data. An analysis of the correlation between the two reported cytotoxic activities shows that r^2[log(GI_{50}), HCT-116- log(GI_{50}), MCF-7]= 0.75.

Table 3. Matrix of squared correlation coefficients for the logarithms of experimental CDK inhibition data.

	CDK9T1	CDK1B	CDK2A
CDK1B	0.67	1.00	
CDK2A	0.72	0.83	1.00
CDK7H	0.07	0.006	0.02

Results for CDK1B inhibition

No statistically significant equation was obtained for the whole set (n=18). Using a methodology that was successful in other cases, we created a new set excluding the molecule with the highest K_i value. For this new set the following equation was obtained:

$$\log(K_i) = 7.29 - 4.03Q_{11}^{\max} + 1.19S_{17}^{E}(HOMO-2)^{*} - 0.08S_{16}^{N}(LUMO)^{*} + 0.50\mu_6 \quad (4)$$

with n=17, F(4,12)=77.51 (p<0.000001), R^2=0.96, adj. R^2=0.95, outliers>2σ=0 and SD=0.12. Here, $Q_{11}^{\max}$ is the maximal charge atom 11 may accept, μ_6 is the local atomic electronic chemical potential of atom 6, $S_{16}^{N}(LUMO)^{*}$ is the local atomic electrophilic superdelocalizability of the lowest vacant molecular orbital (MO) localized on atom 16 and $S_{17}^{E}(HOMO-2)^{*}$ is the local atomic electrophilic superdelocalizability of the third highest occupied MO localized on atom 17 (see Fig. 2). The beta coefficients and *t*-test for the significance of coefficients of Eq. 4 are shown in Table 4. Concerning independent variables, Table 5 shows that there are no significant internal correlations. Figure 3 shows the plot of observed values *vs.* calculated ones.

Table 4. Beta values and results of the t-test for significance of coefficients for the variables appearing in Eq. 4.

	Beta	t(12)	p-level
$Q_{11}^{\max}$	-0.43	-6.17	<0.00004
$S_{17}^{E}(HOMO-2)^{*}$	0.56	9.99	<0.000001
$S_{16}^{N}(LUMO)^{*}$	-0.37	-5.66	<0.0002
μ_6	0.23	3.81	<0.002

Table 5. Matrix of squared correlation coefficients for the variables appearing in Eq. 4.

	$Q_{11}^{\max}$	$S_{17}^{E}(HOMO-2)^{*}$	$S_{16}^{N}(LUMO)^{*}$
$S_{17}^{E}(HOMO-2)^{*}$	0.01	1.00	
$S_{16}^{N}(LUMO)^{*}$	0.24	0.0009	1.00
μ_6	0.10	0.001	0.001

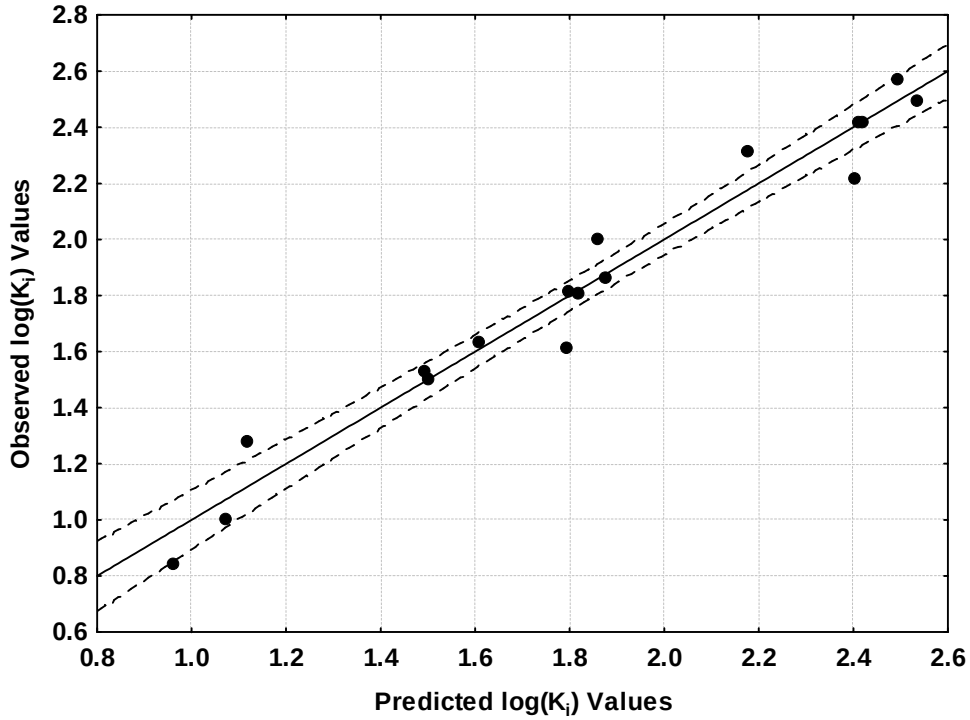

Figure 3. Plot of predicted *vs.* observed log(K_i) values from Eq. 4. Dashed lines denote the 95% confidence interval.

Results for CDK2A inhibition

For this biological activity the following equation was obtained:

$$\log(K_1) = 1.41 + 0.007 S_2^N (LUMO+1)^* - 0.84 S_{18}^E (HOMO-2)^* - 0.04 S_{13}^N (LUMO+2)^* - 2.46 Q_{17} \quad (5)$$

with n=18, F(4,13)=50.64 (p<0.000001), R^2=0.94, adj. R^2=0.92, outliers>2σ=0 and SD=0.19. Here, Q_{17} is the net charge of atom 17, $S_2^N (LUMO+1)^*$ is the local atomic nucleophilic superdelocalizability of the second lowest vacant MO localized on atom 2, $S_{13}^N (LUMO+2)^*$ is the local atomic nucleophilic superdelocalizability of the third lowest vacant MO localized on atom13 and $S_{18}^E (HOMO-2)^*$ is the local atomic electrophilic superdelocalizability of the third highest occupied MO localized on atom 18 (see Fig. 2). The beta coefficients and *t*-test for the significance of coefficients of Eq. 5 are shown in Table 6. Concerning independent variables, Table 7 shows that there are no significant internal correlations. Figure 4 shows the plot of observed values *vs.* calculated ones.

Table 6. Beta values and results of the t-test for significance of coefficients for the variables appearing in Eq. 5.

	Beta	t(13)	p-level
$S_2^N (LUMO+1)^*$	0.72	10.51	<0.000001
$S_{18}^E (HOMO-2)^*$	-0.57	-7.11	<0.000008
$S_{13}^N (LUMO+2)^*$	-0.38	-5.50	<0.0001
Q_{17}	-0.26	-3.26	<0.006

Table 7. Matrix of squared correlation coefficients for the variables appearing in Eq. 5

	$S_2^N(LUMO+1)^*$	$S_{18}^E(HOMO-2)^*$	$S_{13}^N(LUMO+2)^*$
$S_{18}^E(HOMO-2)^*$	0.0009	1.00	
$S_{13}^N(LUMO+2)^*$	0.02	0.008	1.00
Q_{17}	0.005	0.28	0.001

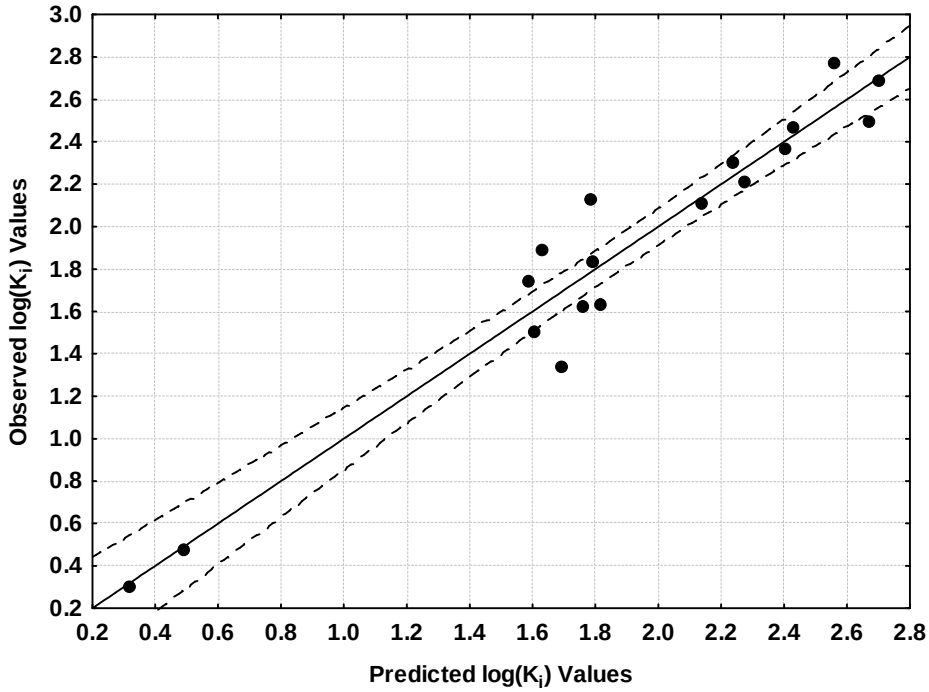

Figure 4. Plot of predicted vs. observed log(K$_i$) values from Eq. 5. Dashed lines denote the 95% confidence interval.

Results for CDK7H inhibition

No statistically significant equation was obtained for the whole set (n=18). We created a new set excluding the four molecules having the highest K_i values. For this new set the following equation was obtained:

$$\log(K_i) = 2.33 + 0.88Q_{18} + 0.01S_5^N(LUMO+1)^* + 0.008S_1^N(LUMO+2)^* + 2.16F_1(HOMO-2)^* \quad (6)$$

with n=14, F(4,9)=23.25 (p<0.00009), R^2=0.91, adj. R^2=0.87, outliers>2σ=0 and SD=0.16. Here, Q_{18} is the net charge of atom 18, $F_1(HOMO-2)^*$ is the electron population of the third highest occupied MO localized on atom 1, $S_5^N(LUMO+1)^*$ is the local atomic nucleophilic superdelocalizability of the second lowest vacant MO localized on atom 5 and $S_1^N(LUMO+2)^*$ is the local atomic nucleophilic superdelocalizability of the third lowest vacant MO localized on atom 1 (see Fig. 2). The beta coefficients and *t*-test for the significance of coefficients of Eq. 6 are shown in Table 8. Concerning independent variables, Table 9 shows that there are no significant internal correlations. Figure 5 shows the plot of observed values *vs.* calculated ones.

Table 8. Beta values and results of the t-test for significance of coefficients for the variables appearing in Eq. 6.

	Beta	t(9)	p-level
Q_{18}	0.40	3.71	<0.005
$S_5^N(LUMO+1)*$	0.47	4.63	<0.001
$S_1^N(LUMO+2)*$	0.43	4.25	<0.002
$F_1(HOMO-2)*$	0.35	3.39	<0.008

Table 9. Matrix of squared correlation coefficients for the variables appearing in Eq. 6.

	Q_{18}	$S_5^N(LUMO+1)*$	$S_1^N(LUMO+2)*$
$S_5^N(LUMO+1)*$	0.04	1.00	
$S_1^N(LUMO+2)*$	0.03	0.0009	1.00
$F_1(HOMO-2)*$	0.08	0.006	0.0009

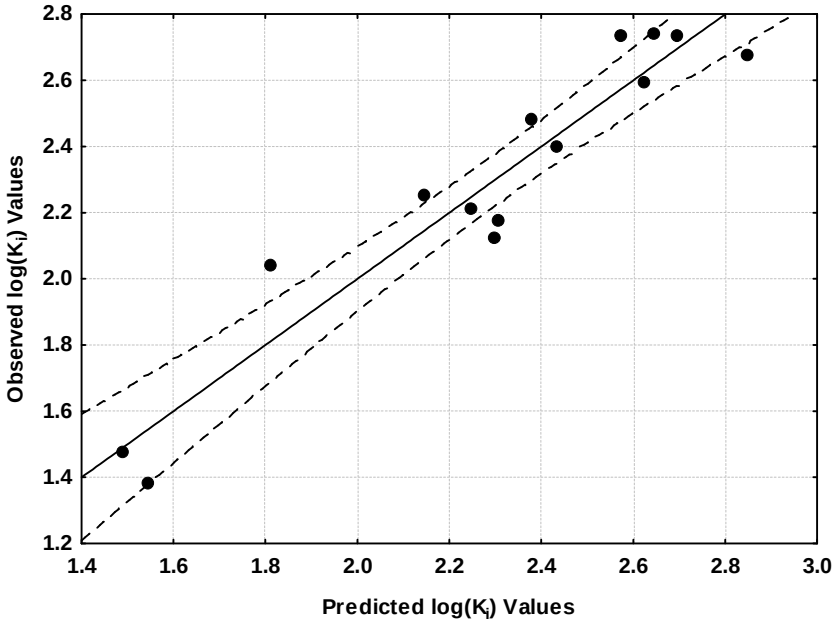

Figure 5. Plot of predicted *vs.* observed log(K_i) values from Eq. 6. Dashed lines denote the 95% confidence interval.

Results for CDK9T1 inhibition

For this biological activity the following equation was obtained:

$$\log(K_i) = 2.29 - 0.03S_{16}^N(LUMO)* - 0.04S_9^N(LUMO+2)* - 3.32F_{16}(LUMO+1)* + \\ +0.96S_{17}^E(HOMO-2)* + 1.74S_9^E(HOMO-2)* \quad (7)$$

with n=19, F(5,13)=54.86 (p<0.000001), R^2=0.95, adj. R^2=0.94, outliers>2σ=0 and SD=0.14. Here, $F_{16}(LUMO+1)*$ is the electron population of the second lowest vacant MO localized on atom 16, $S_{16}^N(LUMO)*$ is the local atomic nucleophilic superdelocalizability of the lowest vacant MO localized on atom 16, $S_{17}^E(HOMO-2)*$ is the local atomic electrophilic superdelocalizability of the third highest occupied MO

localized on atom 17, $S_9^N(LUMO+2)*$ is the local atomic nucleophilic superdelocalizability of the third lowest MO localized on atom 9 and $S_9^E(HOMO-2)*$ is the local atomic electrophilic superdelocalizability of the third highest MO localized on atom 9 (see Fig. 2). The beta coefficients and *t*-test for the significance of coefficients of Eq. 7 are shown in Table 10. Concerning independent variables, Table 11 shows that there are no significant internal correlations. Figure 6 shows the plot of observed values *vs.* calculated ones.

Table 10. Beta values and results of the t-test for significance of coefficients for the variables appearing in Eq. 7.

	Beta	t(13)	p-level
$S_{16}^N(LUMO)*$	-0.39	-5.31	<0.0001
$S_9^N(LUMO+2)*$	-0.63	-8.28	<0.000002
$F_{16}(LUMO+1)*$	-0.63	-7.27	<0.000006
$S_{17}^E(HOMO-2)*$	0.41	6.36	<0.00003
$S_9^E(HOMO-2)*$	0.30	4.45	<0.0007

Table 11. Matrix of squared correlation coefficients for the variables appearing in Eq. 7.

	$S_{17}^E(HOMO-2)*$	$S_{16}^N(LUMO)*$	$F_{16}(LUMO+1)*$	$S_{17}^E(HOMO-2)*$
$S_{16}^N(LUMO)*$	0.02	1.00		
$F_{16}(LUMO+1)*$	0.14	0.36	1.00	
$S_{17}^E(HOMO-2)*$	0.03	0.04	0.07	1.00
$S_9^E(HOMO-2)*$	0.12	0.0009	0.01	0.06

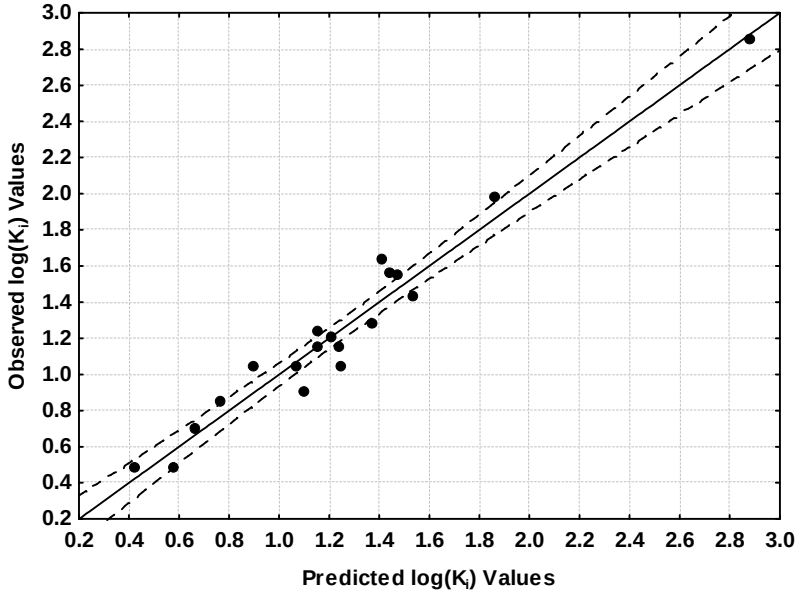

Figure 6. Plot of predicted *vs.* observed log(K_i) values from Eq. 7. Dashed lines denote the 95% confidence interval.

Results for anti-proliferative activity against human colon cancer HCT-116 cells
For this biological activity the following equation was obtained:

$$\log(GI_{50}) = -3.35 + 0.009O_{R1} + 0.37\eta_{16} - 0.65S_1^E(HOMO-1)* - \\ -3.15F_{17}(HOMO-1)* - 0.12S_{12}^E(HOMO-2)* \quad (8)$$

with n=19, F(5,13)=17.06 (p<0.00003), R^2=0.87, adj. R^2=0.82, outliers>2σ=0 and SD=0.20. Here, O_{R1} is the orientational parameter of the R_1 substituent, η_{16} is the local atomic hardness of atom 16, $F_{17}(HOMO-1)*$ is the electron population of the second highest MO localized on atom 17, $S_1^E(HOMO-1)*$ is the local atomic electrophilic superdelocalizability of the second highest MO localized on atom 1 and $S_{12}^E(HOMO-2)*$ is the local atomic electrophilic superdelocalizability of the third highest MO localized on atom 12 (see Fig. 2). The beta coefficients and *t*-test for the significance of coefficients of Eq. 8 are shown in Table 12. Concerning independent variables, Table 13 shows that there are no significant internal correlations. Figure 7 shows the plot of observed values *vs.* calculated ones.

Table 12. Beta values and results of the t-test for significance of coefficients for the variables appearing in Eq. 8.

	Beta	t(13)	p-level
O_{R1}	0.69	6.50	<0.00002
η_{16}	0.25	2.28	<0.04
$S_1^E(HOMO-1)*$	-0.43	-3.90	<0.002
$F_{17}(HOMO-1)*$	-0.42	-3.51	<0.004
$S_{12}^E(HOMO-2)*$	-0.31	-2.56	<0.02

Table 13. Matrix of squared correlation coefficients for the variables appearing in Eq. 8.

	O_{R1}	η_{16}	$S_1^E(HOMO-1)*$	$F_{17}(HOMO-1)*$
η_{16}	0.04	1.00		
$S_1^E(HOMO-1)*$	0.03	0.09	1.00	
$F_{17}(HOMO-1)*$	0.02	0.03	0.001	1.00
$S_{12}^E(HOMO-2)*$	0.002	0.003	0.03	0.22

Results for anti-proliferative activity against human breast cancer MCF-7 cells
For this biological activity the following equation was obtained:

$$\log(GI_{50}) = 9.00 + 25.87Q_{15} - 0.32\eta_1 + 4.64F_{15}(HOMO-1)* + 0.005S_{16}^N(LUMO+2)* - \\ -1.88F_{12}(HOMO)* - 22.86s_3 \quad (9)$$

with n=19, F(6,12)=48.74 (p<0.00001), R^2=0.96, adj. R^2=0.94, outliers>2σ=0 and SD=0.09. Here, Q_{15} is the net charge of atom 15, η_1 is the local atomic hardness of atom 1, s_3 is the local atomic softness of atom 3, $F_{15}(HOMO-1)*$ is the electron population of the second highest occupied MO localized on atom 15, $F_{12}(HOMO)*$ is the electron population of the highest occupied MO localized on atom 12 and $S_{16}^N(LUMO+2)*$ is the local atomic nucleophilic superdelocalizability of the third lowest vacant MO localized on atom 16 (see Fig. 2). The beta coefficients and *t*-test for the significance of coefficients of Eq. 9 are shown in

Table 14. Concerning independent variables, Table 15 shows that there are no significant internal correlations. Figure 8 shows the plot of observed values *vs.* calculated ones.

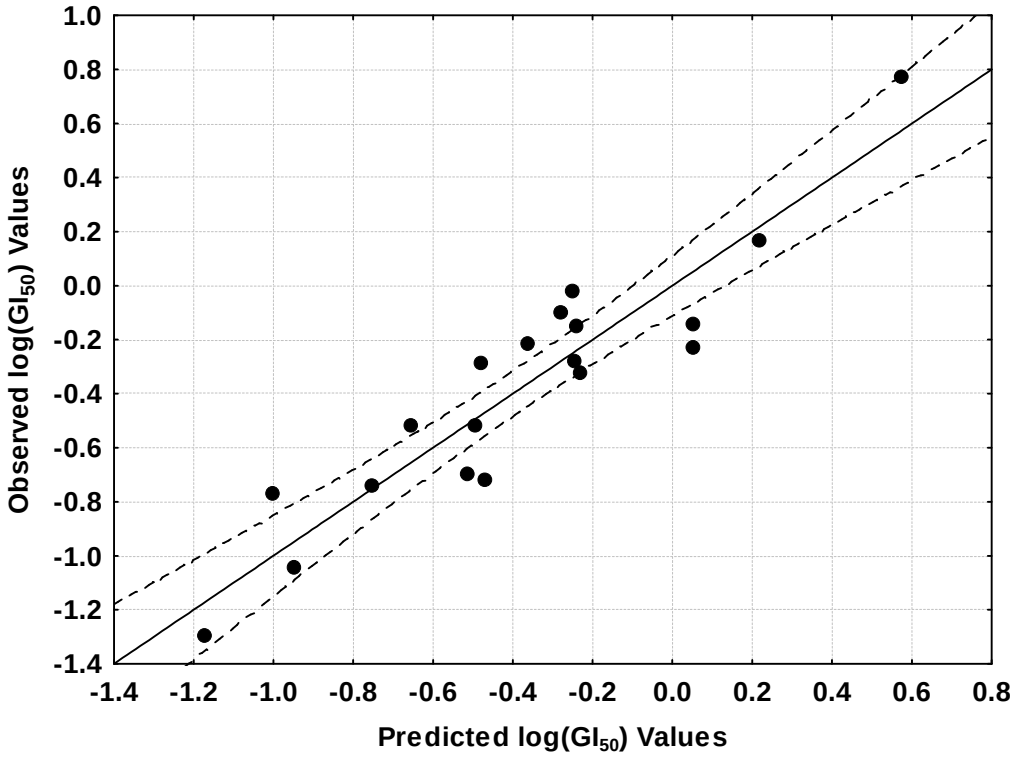

Figure 7. Plot of predicted *vs.* observed log(GI_{50}) values from Eq. 8. Dashed lines denote the 95% confidence interval.

Table 14. Beta values and results of the t-test for significance of coefficients for the variables appearing in Eq. 9.

	Beta	t(12)	p-level
Q_{15}	0.86	11.17	<0.000001
η_1	-0.63	-9.11	<0.00001
$F_{15}(HOMO-1)*$	0.74	9.55	<0.00001
$S_{16}^{N}(LUMO+2)*$	0.57	7.17	<0.00001
$F_{12}(HOMO)*$	-0.37	-4.62	<0.0006
s_3	-0.21	-2.97	<0.01

Table 15. Matrix of squared correlation coefficients for the variables appearing in Eq. 9.

	Q_{15}	η_1	$F_{15}(HOMO-1)*$	$S_{16}^{N}(LUMO+2)*$	$F_{12}(HOMO)*$
η_1	0.04	1.00			
$F_{15}(HOMO-1)*$	0.0009	0.0009	1.00		
$S_{16}^{N}(LUMO+2)*$	0.14	0.06	0.15	1.00	
$F_{12}(HOMO)*$	0.16	0.008	0.14	0.004	1.00
s_3	0.02	0.27	0.006	0.02	0.02

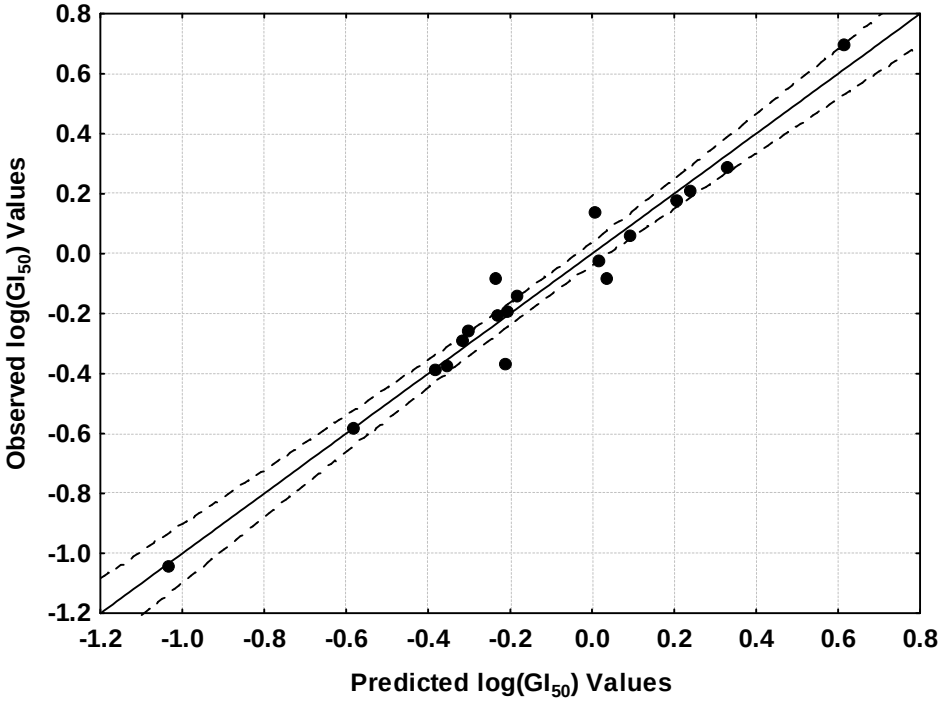

Figure 8. Plot of predicted *vs.* observed log(IG_{50}) values from Eq. 9. Dashed lines denote the 95% confidence interval

DISCUSSION

CDK1B inhibition

The associated statistical parameters of Eq. 4 show that this equation is statistically significant and that the variation of a group of local atomic reactivity indices belonging to the common skeleton shown in Fig. 2 explains about 95% of the variation of the inhibitory activity against CDK1B. The beta values (Table 4) show that the relative importance of these indices is $S_{17}^{E}(HOMO-2)^{*} > Q_{11}^{\max} > S_{16}^{N}(LUMO)^{*} > \mu_6$. A high CDK1B inhibitory capacity is associated with high values for $S_{17}^{E}(HOMO-2)^{*}$ and $Q_{11}^{\max}$, with a small value for $S_{16}^{N}(LUMO)^{*}$ and with negative values for μ_6. The local $(HOMO-2)_{17}$* (atom 17 is located in ring C, see Fig. 2) is of π nature in all molecules. Fig. 9 shows, for example, the local $(HOMO-2)_{17}$* of molecules 2 and 9.

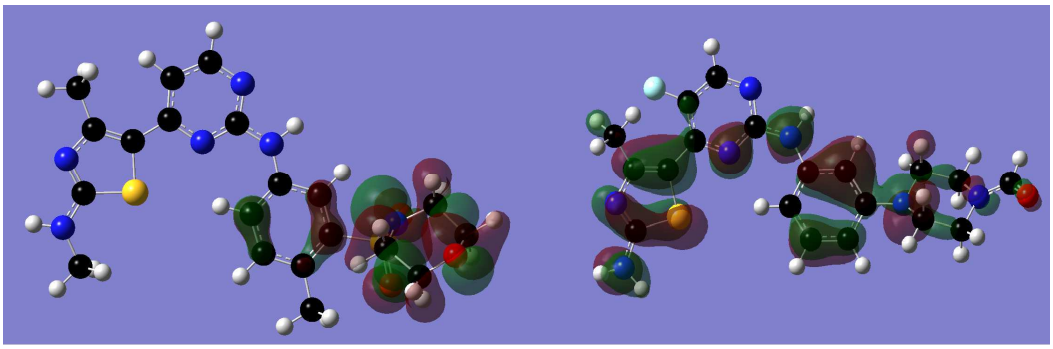

Figure 9. Local $(HOMO-2)_{17}$* in molecules 9 (left) and 2 (right).

Considering that $(HOMO-1)_{17}$* and $HOMO_{17}$* are also of π nature, we suggest that the three highest occupied local MOs of atom 17 are interacting with a moiety of the binding site having several vacant π MOs. Atom 11, carbon one (see Fig. 2), is surrounded by three nitrogen atoms and has a positive net charge. A high Q_{11}^{max} value suggests that this atom should be able to receive the maximal amount of charge possible. Then, atom 11 seems to participate as an electron-acceptor in a charge-transfer process possibly through a π-π* stacking. In closed-shell, fully saturated molecules, μ_6 should be always negative. Atom 6 is a methyl carbon atom. To obtain a higher value we need to shift the local $HOMO_6$* energy downwards, making atom 6 a bad electron donor. In the case of this sp^3 carbon atom, we propose that it is interacting with a region of the CDK1B binding site having filled σ molecular orbitals (such as an alkyl chain). A small value of $S_{16}^N(LUMO)*$ is required for optimal activity. The eigenvalue of $LUMO_{16}$* is negative and the OM is of π nature. A small value for $S_{16}^N(LUMO)*$ can be obtained by shifting the eigenvalue downwards and making atom 16 a good electron acceptor. Therefore we suggest that atom 16 is interacting with a π electron-donor region of the CDK1B binding site. Note the fact that atoms 16 and 17 are mutually bonded, that they belong to an aromatic moiety and that they act in opposite ways (atom 16 as an electron-acceptor and atom 17 as an electron-donor). This could be an indication that ring C is participating as such in a π-π stacking with a complementary aromatic locus of the CDK1B binding site. All these ideas are depicted in the partial two-dimensional (2D) for CDK1B inhibition shown in Fig. 10.

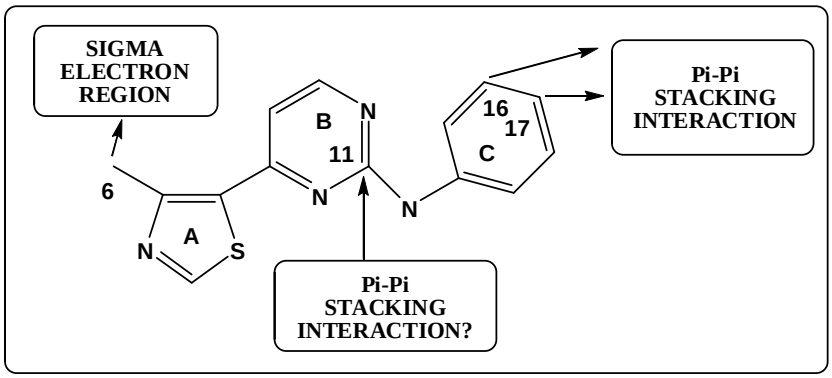

Figure 10. Partial 2D pharmacophore for the inhibition of CDK1B.

CDK2A inhibition

The associated statistical parameters of Eq. 5 show that this equation is statistically significant and that the variation of a group of four local atomic reactivity indices belonging to the common skeleton shown in Fig. 2 explains about 92% of the variation of the inhibitory activity against CDK2A. The beta values (Table 6) show that the relative importance of these indices is $S_2^N(LUMO+1)*$ > $S_{18}^E(HOMO-2)*$ > $S_{13}^N(LUMO+2)*$ > Q_{17} (see Fig. 2). A high CDK2A inhibitory capacity is associated with high values for Q_{17} (if positive) and with a small value for $S_{18}^E(HOMO-2)*$ (which is always negative**).** The requirements for $S_2^N(LUMO+1)*$ and $S_{13}^N(LUMO+2)*$ depend on the sign of their values. This is so because Hartree-Fock and DFT calculations produce vacant molecular orbitals with negative or positive eigenvalues. When the value of $S_2^N(LUMO+1)*$ is negative, high negative numerical values are required for best activity. This can be achieved by shifting the local MO energy *upwards*. When the value of $S_2^N(LUMO+1)*$ is positive, low numerical values are required. This is obtained also by shifting the local MO energy *upwards*. Another way to fulfill the requirements is by lowering the values of the associated Fukui indices. $(LUMO)_2$* and $(LUMO+1)_2$* are local π MOs in all the molecules. Then we may hypothesize that the presence of $(LUMO+1)_2$* is hindering a π*-π interaction of atom 2 with a counterpart in the CDK2A binding site. As the numerical values of $S_{13}^N(LUMO+2)*$ (atom 13 is a nitrogen atom) can also be positive or negative, a similar analysis can be carried out. Considering that in this case the $(LUMO+2)_{13}$* local MO

energy should be shifted *downwards* and that this local MO is of π nature ($(LUMO)_{13}$* and $(LUMO+1)_{13}$* also have π nature), we propose that this atom interacts with an electron-rich counterpart in the CDK2A binding site. It is highly possible that this interaction occurs through a hydrogen bond. Atom 17 should have a positive net charge for optimal inhibition, suggesting an electrostatic interaction with a negatively charged moiety located in the CDK2A binding site. The local $(HOMO-2)_{18}$* is of π nature in all the molecules. A small value for $S_{18}^{E}(HOMO-2)$* could indicate that this local MO is hindering the interaction of the two highest occupied MOs (that are of π nature) with a π electron-deficient moiety in the CDK2A binding site. All these suggestions are presented in the partial 2D inhibition pharmacophore shown in Fig. 11.

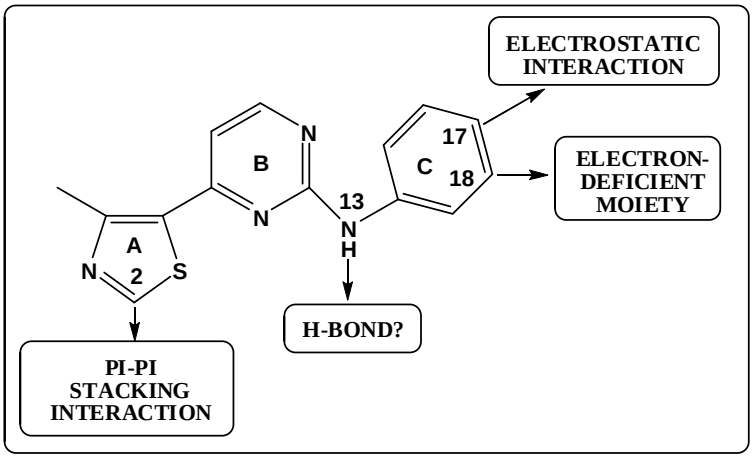

Figure 11. Partial 2D pharmacophore for the inhibition of CDK2A.

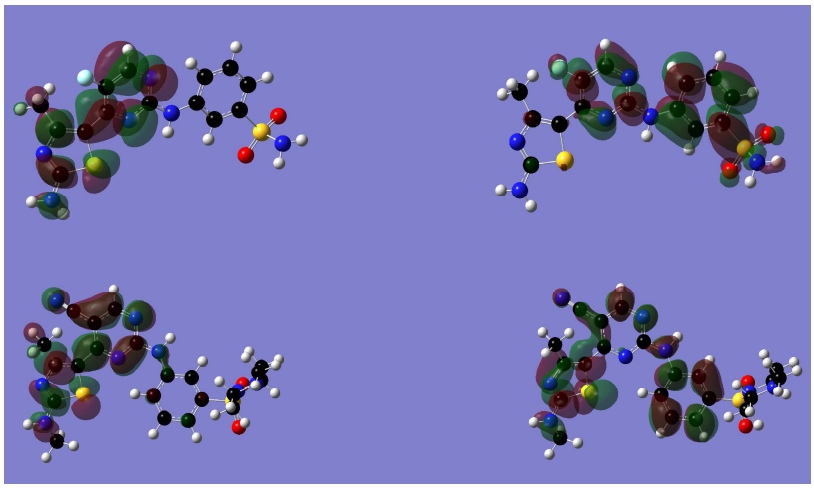

Figure 12. Local $(LUMO)_5$* (left) and $(LUMO+1)_5$* (right) of molecules 1 (upper) and 11 (lower).

CDK7H inhibition

The associated statistical parameters of Eq. 6 show that this equation is statistically significant and that the variation of a group of four local atomic reactivity indices belonging to the common skeleton shown in Fig. 2 explains about 87% of the variation of the inhibitory activity against CDK7H. The beta values (Table 8) show that the relative importance of these indices is $S_5^N(LUMO+1)^* > S_1^N(LUMO+2)^* > Q_{18} > F_1(HOMO-2)^*$ (see Fig. 2). A high CDK7H inhibitory capacity is associated with high values for Q_{18} (if negative) and with a small value for $F_1(HOMO-2)^*$. The requirements for $S_5^N(LUMO+1)^*$ and $S_1^N(LUMO+2)^*$ depend on the sign of

their values. Atom 18 belongs to ring C. A negative charge suggests an electrostatic interaction of atom 18 with a positively charged counterpart in the CDK7H binding site. Atom 5 is a carbon belonging to ring A (see Fig. 2). An optimal value for $S_5^N(LUMO+1)^*$ for a good CDK7H inhibition demands that the $(LUMO+1)_5^*$ energy be shifted upwards or that the associated Fukui index be lowered (a combination of both conditions also works, but we must remember that the Fukui index should be always greater than zero). We may speculate then that $(LUMO+1)_5^*$ could be participating in a repulsive (zero electron) interaction with a vacant MO located in the CDK7H binding site. On the other hand, $(LUMO)_5^*$ has π nature in all molecules. Figure 12 shows, for example, the local $(LUMO)_5^*$ and $(LUMO+1)_5^*$ for molecules 1 and 11.

We can see that $(LUMO)_5^*$ of both molecules is part of a large π MO localized on rings A and B (see Fig. 2). In the case of molecule 1 the local $(LUMO+1)_5^*$ (upper right) has a very small localization on atom 5, while in molecule 11 (lower right) it has a much more noticeable localization on that atom (and on ring A). Then, $(LUMO)_5^*$ seems to participate in an interaction with an electron-rich area. Equation 6 contains two local atomic reactivity indices belonging to atom 1: $S_1^N(LUMO+2)^*$ and $F_1(HOMO-2)^*$. They are not correlated (see Table 9), $S_1^N(LUMO+2)^*$ having a higher beta value than $F_1(HOMO-2)^*$ (Table 8). $(HOMO-2)_1^*$ is of σ nature. A small value suggests that $(HOMO-1)_1^*$ and $(HOMO)_1^*$, both of π nature, are interacting with an electron-deficient center located in the CDK7H binding site and that $(HOMO-2)_1^*$ seems to be engaged in a repulsive interaction with occupied σ or π MOs. $(LUMO+2)_1^*$ is of σ nature. For optimal activity, this index should be small. Considering that $(LUMO+1)_1^*$ and $(LUMO)_1^*$ are of π nature this should indicate that atom 1 is interacting with an electron-rich center in the CDK7H binding site. It seems that there is a contradiction with the previous suggestion for the role of atom 1. Without more experimental data to analyze we have two possible solutions for this. The first is to simply consider only $S_1^N(LUMO+2)^*$ for the analysis because of its higher beta value. The second is to suggest that atom 1, a nitrogen atom of ring A, is really participating in the interaction with two different *loci* in a sandwiched position. All the above ideas are shown in the partial two-dimensional (2D) inhibition pharmacophore shown in Fig. 13.

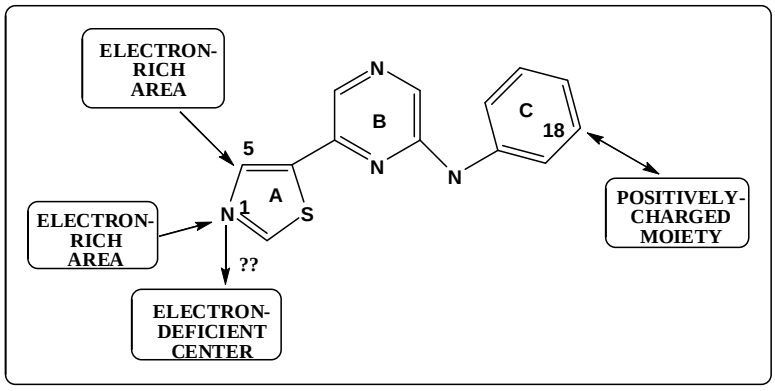

Figure 13. Partial 2D pharmacophore for the inhibition of CDK7H.

CDK9T1 inhibition

The associated statistical parameters of Eq. 7 show that this equation is statistically significant and that the variation of a group of five local atomic reactivity indices belonging to the common skeleton shown in Fig. 2 explains about 94% of the variation of the inhibitory activity against CDK9T1. The beta values (Table 10) show that the relative importance of these indices is $S_9^N(LUMO+2)^* = F_{16}(LUMO+1)^* > S_{17}^E(HOMO-2)^* > S_{16}^N(LUMO)^* > S_9^E(HOMO-2)^*$. A high CDK9T1 inhibitory capacity is associated with high values for $S_{17}^E(HOMO-2)^*$, $S_9^E(HOMO-2)^*$ and $F_{16}(LUMO+1)^*$. In the case of

$S_9^N(LUMO+2)^*$ and $S_{16}^N(LUMO)^*$, a high value is needed if they are positive and if negative a small value is required**.** A high value for $F_{16}(LUMO+1)^*$ ($(LUMO+1)_{16}{}^*$ is of π nature) suggests that atom 16 is interacting with an electron-rich center located in the CDK9T1 binding site. In this interaction $(LUMO)_{16}{}^*$, a π MO, also participates. A high value for $S_9^E(HOMO-2)^*$ ($(HOMO-2)_9{}^*$ is a π MO) indicates that atom 9 is interacting with an electron-deficient center located in the CDK9T1 binding site through $(HOMO-2)_9{}^*$, $(HOMO-1)_9{}^*$ and $(HOMO)_9{}^*$. The same holds for atom 17: it interacts with an electron-deficient center through its first two highest local occupied MOs (both of π nature). In the case of $S_9^N(LUMO+2)^*$ and $S_{16}^N(LUMO)^*$ optimal activity is associated with a lowering of the respective vacant MO energies. For $S_{16}^N(LUMO)^*$ this means that the electron-accepting properties of this local MO are enhanced and that atom 16 is interacting with an electron-rich center located in the CDK9T1 binding site, a fact that is fully consistent with the requirements for $F_{16}(LUMO+1)^*$ (see above). For $S_9^N(LUMO+2)^*$, the situation is analogous. $(LUMO+2)_9{}^*$ is a π MO. Then atom 9 seems to interact with an electron-rich center located in the CDK9T1 binding site through its first three vacant local MOs. All the above ideas are shown in the partial 2D inhibition pharmacophore shown in Fig. 14.

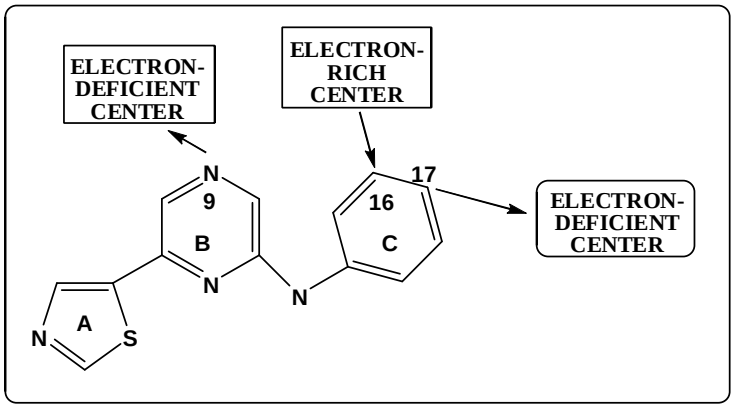

Figure 14. Partial 2D pharmacophore for the inhibition of CDK9T1.

Anti-proliferative activity against human colon cancer HCT-116 cells

The associated statistical parameters of Eq. 8 show that this equation is statistically significant and that the variation of the value of four local atomic reactivity indices belonging to the common skeleton shown in Fig. 2, plus the orientational parameter of the R_1 substituent explain about 82% of the variation of the anti-proliferative activity against HCT-116 cells. The beta values (Table 12) show that the relative importance of these indices is O_{R1} > $S_1^E(HOMO-1)^*$ > $F_{17}(HOMO-1)^*$ > $S_{12}^E(HOMO-2)^*$ > η_{16}. A high antiproliferative activity is associated with high values for $F_{17}(HOMO-1)^*$, and with small values for O_{R1}, $S_1^E(HOMO-1)^*$, $S_{12}^E(HOMO-2)^*$ and η_{16} (see Fig. 2)**.** Table 1 shows that the R_1 substituent is NH_2 or NHMe. A low value for the orientational parameter, that is a purely geometric index, suggests that the NH_2 group seems to be optimal. We can substitute NH_2 with a substituent having a lower OP value provided that its electronic effects on the ring system are the same. Atom 12 is a nitrogen belonging to ring B. $(HOMO-2)_{12}{}^*$ is of σ nature in almost all the molecules. A small value for $S_{12}^E(HOMO-2)^*$ can be obtained by shifting the MO energy downwards and/or by lowering the corresponding Fukui index (this last index is always greater than zero). This

suggests that atom 12 is interacting with an electron-deficient center in the binding site through its $(HOMO)_{12}$*. $(HOMO-2)_{12}$* seems to be participating in a repulsive interaction with an occupied MO of the binding site. Considering that in some molecules $(HOMO-2)_{12}$* is of σ nature while in others it is π, an optimal situation should be when the two highest occupied local MOs are of π nature and the third highest occupied MO is of σ nature but well down along the energy axis. $S_1^E(HOMO-1)$* should be small. Atom 1 is the nitrogen belonging to ring A. $(HOMO-1)_1$* is a π MO. We suggest that atom 1 is interacting with an electron-deficient center through its $(HOMO)_1$* only. This interaction could be of the MO-MO kind or a hydrogen bond. A high value for $F_{17}(HOMO-1)$* suggests that atom 17 is interacting with an electron-deficient center in the binding site through its $(HOMO-1)_{17}$* and $(HOMO)_{17}$*. η_{16} will not be discussed because of its low p-level (Table 12). All the above ideas are shown in the partial 2D inhibition pharmacophore shown in Fig. 15.

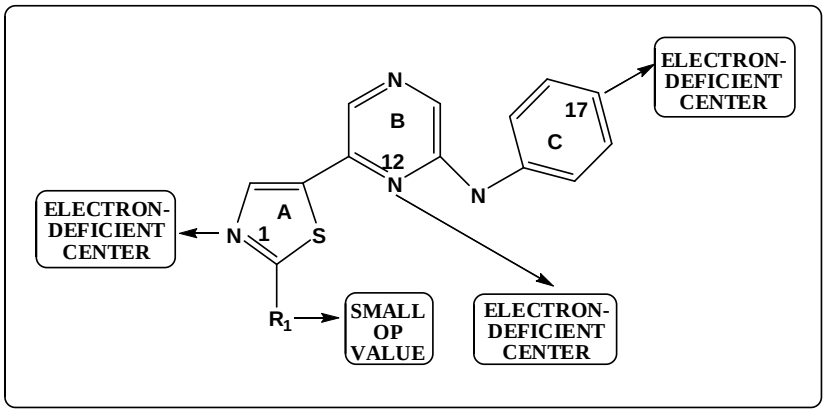

Figure 15. Partial 2D pharmacophore for the anti-proliferative activity against human colon cancer HCT-116 cells.

The small number of reactivity indices appearing in Eq. 8, together with the high degree of orbital control (including the inner occupied and higher vacant MOs), seems to indicate that these molecules all the same mechanism of action and their site of action is a *locus* directly related to the proliferative process of HCT-116 cells.

Anti-proliferative activity against human breast cancer MCF-7 cells

The associated statistical parameters of Eq. 9 show that this equation is statistically significant and that the variation of a group of six local atomic reactivity indices belonging to the common skeleton shown in Fig. 2 explains about 94% of the variation of the anti-proliferative activity against MCF-7 cells. The beta values (Table 14) show that the relative importance of these indices is Q_{15} > $F_{15}(HOMO-1)$* > η_1 > $S_{16}^N(LUMO+2)$* > $F_{12}(HOMO)$* > s_3 (see Fig. 2). High antiproliferative activity is then associated with high values for η_1 and $F_{12}(HOMO)$*, with small values for $F_{15}(HOMO-1)$*, with negative values for Q_{15} and with small values for $S_{16}^N(LUMO+2)$* if positive. A negative net charge of atom 15, a carbon atom of ring C, indicates the existence of an electrostatic interaction with a positively-charged moiety. A high value for η_1 is indicating that atom 1 (the nitrogen atom of ring A) resists exchanging electrons with the environment. This, in turn, suggests that atom 1 is probably located close to a hydrophobic moiety (an alkyl chain for example). Note that here atom 1 plays a different role than in HCT-116 cells. A high value for $F_{12}(HOMO)$* suggests that atom 12 is interacting with an electron-deficient center through its $(HOMO)_{12}$*, a π MO. A low value for $F_{15}(HOMO-1)$* indicates that atom 15 is interacting with an electron-deficient center through its $(HOMO)_{15}$*, a π MO. $(HOMO-1)_{15}$*, also a π MO, seems to participate in a repulsive interaction with at least one occupied MO of the same moiety. $S_{16}^N(LUMO+2)$* needs

to be small. $(LUMO+2)_{16}$* is a π MO. Considering that $(LUMO)_{16}$* and $(LUMO+1)_{16}$* are also π MOs, we suggest that atom 16 is interacting with an electron-rich moiety through its two lowest vacant MOs, and that the third lowest vacant orbital is participating in a repulsive interaction with an empty MO of the moiety. s_3 will not be discussed because of its low p-level. All the above ideas are shown in the partial 2D inhibition pharmacophore shown in Fig. 16.

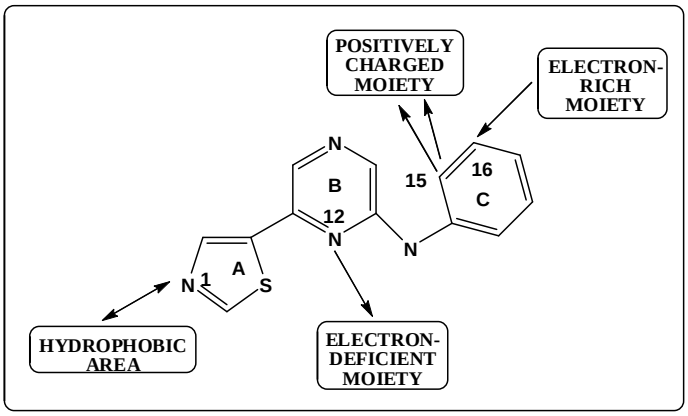

Figure 16. Partial 2D pharmacophore for the anti-proliferative activity against human colon cancer MCF-7 cells.

In a similar way to the anti-proliferative activity against human HCT-116 cells, the results seem to indicate that these molecules have all the same action mechanism and their site of action is a *locus* belonging to the MCF-7 cell replication machine, consistent with the function of the CDKs.

Conformational aspects

Figure 17 shows the ten lowest energy conformers of molecule 1 obtained with MarvinView (Dreiding Force Field) and superimposed with Hyperchem [114, 115].

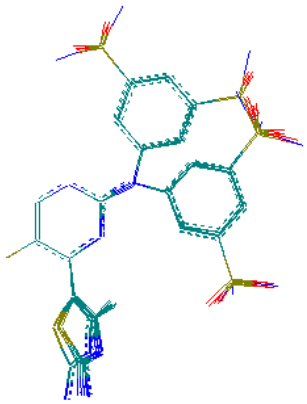

Figure 17. Superimposition of the ten lowest energy conformers of molecule 1.

We can see that ring C (see Fig. 2) can adopt two alternative conformations with respect to rings A-B. The exact conformation or conformations existing during the interaction with the enzymes is not known. The important fact is that if the nitrogen atom joining rings B and C is involved in a hydrogen bond through its hydrogen atom, the direction of this bond cannot be determined with our method. In fact, in the fully optimized geometry of molecules 1 and 2 ring the corresponding N13-H systems point in different directions as shown in Fig. 18.

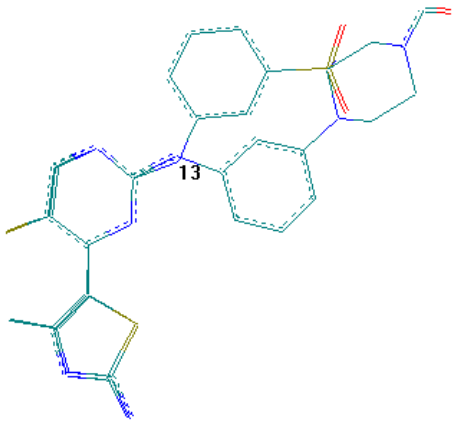

Figure 18. Superimposition of molecules 1 and 2. The number 13 denotes the N atom joining rings B and C.

Molecular electrostatic potential

The molecular electrostatic potential map can provide information about the side (or sides) from which the molecules approach their action site. Figures 18 and 19 show the MEP map of molecules 1, 2, 7 and 11 at 4.5 Å of their nuclei.

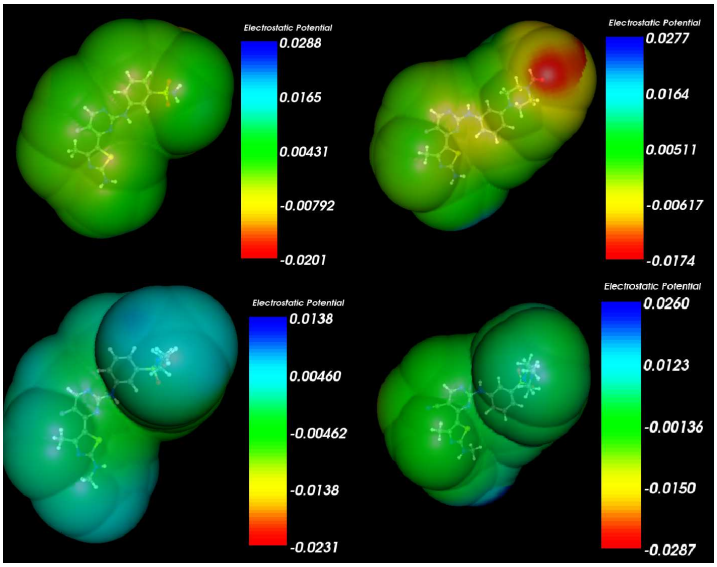

Figure 18. MEP map of molecules 1 (upper left), 2 (upper right), 7 (lower left) and 11 (lower right) at 4.5 Å of the nuclei.

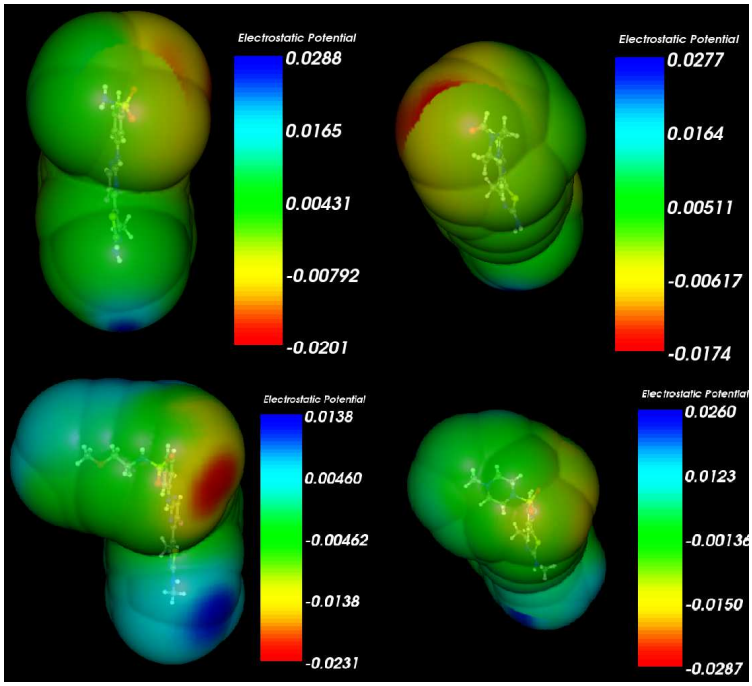

Figure 19. MEP map of molecules 1 (upper left), 2 (upper right), 7 (lower left) and 1 (lower right) at 4.5 Å from the nuclei.

We can see that in molecules 1 and 7 the aforementioned N13-H system points in one direction while in molecules 2 and 11 it is pointing in another. A positive MEP area surrounds rings A and B (see Fig. 2). The MEP structure around ring C depends on the structure and size of its substituents. Fig. 19 shows that the most positive MEP areas are located close to the R_1 substituent. It is then possible to suggest that these molecules point their ring A toward the site while approaching it. The different position of the N13-H system does not alter the MEP structure around ring A. Figure 20 shows the MEP map of the same molecules for surfaces with isovalues of ±0.01.

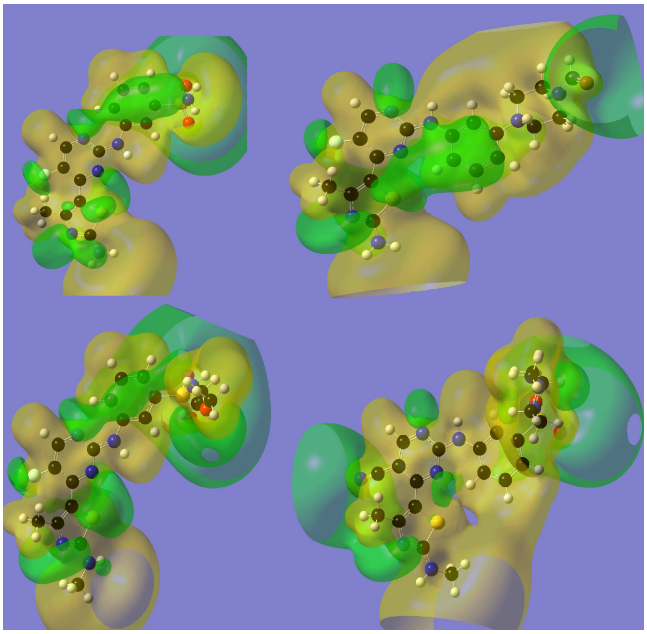

Figure 20. MEP map of molecules 1 (upper left), 2 (upper right), 7 (lower left) and 11 (lower right). The green isovalue surface corresponds to negative MEP values (-0.01) and the yellow isovalue surface to positive MEP values (0.01).

This analysis of the MEP map at a short distance should help to get a deeper understanding of the proposed partial pharmacophores. It is worth mentioning that this kind of analysis is only qualitative because the MEP will undergo a deformation at a short distance due to the molecule-site interactions. We suggest that, if rings A-B-C are placed in the same relative position in all molecules, then there should be a relationship between the MEP structure and the pharmacophores' features. In this case, and due to the two possible positions of N13-H, this analysis is not directly achievable with the data obtained here. Nevertheless, considering that in docking studies the proton of N13 (see Fig. 2 for atom numbering) is always placed on the opposite side to the sulphur atom of ring A [40], we shall employ the MEP maps of molecules 2 and 11 as a basis for the ensuing examples. In the case of the partial 2D pharmacophore for CDK1B inhibition it is suggested that the C6 methyl carbon could interact with occupied σ MOs belonging to the binding site. This proposed site should have a positive MEP region around it and, as the C6 methyl carbon has a positive MEP area around it, this interaction should be repulsive. C11 has a positive MEP around it. Then, if it is involved in a π-π stacking interaction, it must face a carbon atom surrounded by a negative MEP area. In the case of ring C a finer discussion is hindered because of the MEP structure around it, but it is possible to suggest that this ring is not fully involved in a stacking interaction and that only atoms 16 and 17 participate in it. Another example involves the possible participation of the N13-H moiety in a H-bond. The hydrogen atom is surrounded by a positive MEP area allowing it to be shared with an oxygen atom (that almost always has a negative MEP area around it) belonging to the binding site. In the case of N1, the partial 2D pharmacophore suggests that it could be interacting with an electron-rich center, an electron-deficient center or both. The negative MEP area around it supports the second suggestion with the possibility that the electron-deficient center be a hydrogen atom (to form a H-bond) or a positively charged moiety.

CONCLUSION

We found statistically significant relationships between the electronic structures of a series of 2,4,5-trisubstituted pyrimidines and their ability to inhibit four cyclin-dependent kinases. Also we found relationships between the electronic structures and anti-proliferative activities against the MCF-7 and HCT-116 cell lines. The corresponding partial pharmacophores were proposed and discussed. In the case of the anti-proliferative action against MCF-7 and HCT-116 cell lines, the results strongly suggest that all the molecules studied here have the same mechanism of action mechanism against each cell line and that their site of action is located somewhere in the cell replication mechanism.

Acknowledgements
Prof. Dr. Bruce K. Cassels (Faculty of Sciences, University of Chile) is thanked for helpful comments.

REFERENCES

[1]. AD Wells; PA Morawski, *Nat Rev Immunol*, **2014**, 14, 261-270.
[2]. J Lee; N Yun; C Kim; M-Y Song; K-S Park; YJ Oh, *Biochem. Biophys. Res. Comm.*, **2014**, 447, 121-127.
[3]. YJ Choi; L Anders, *Oncogene*, **2014**, 33, 1890-1903.
[4]. Y Yang; H Wang; J Zhang; F Luo; K Herrup, et al., *Dev. Biol.*, **2013**, 378, 94-106.
[5]. C Trovesi; N Manfrini; M Falcettoni; MP Longhese, *J. Mol. Biol.*, **2013**, 425, 4756-4766.
[6]. Laura A Simmons Kovacs; Michael B Mayhew; David A Orlando; Y Jin; Q Li, et al., *Molec. Cell*, **2013**, 49, 1177-1179.
[7]. L Qiao; P Paul; S Lee; J Qiao; Y Wang; DH Chung, *Biochem. Biophys. Res. Comm.*, **2013**, 435, 295-299.
[8]. M Nishigaki; Y Kawada; T Misaki; K Murata; T Goshima, et al., *Biochem. Biophys. Res. Comm.*, **2013**, 432, 654-659.
[9]. A Kumazawa; N Mita; M Hirasawa; T Adachi; H Suzuki, et al., *Mol. Cell. Neurosci.*, **2013**, 52, 97-105.
[10]. JA Endicott; MEM Noble, *Biochem Soc Trans*, **2013**, 41, 1008-1016.
[11]. A Camins; JG Pizarro; J Folch, "Cyclin-Dependent Kinases," in *Brenner's Encyclopedia of Genetics (Second Edition)*, S. Maloy, and K. Hughes Eds., pp. 260-266, Academic Press, San Diego, 2013.
[12]. T Ye; AKY Fu; NY Ip, "Chapter Five - Cyclin-Dependent Kinase 5 in Axon Growth and Regeneration," in *International Review of Neurobiology*, L. G. Jeffrey, and F. T. Ephraim Eds., vol. Volume 105, pp. 91-115, Academic Press, 2012.
[13]. F Uhlmann; C Bouchoux; S López-Avilés, *Phil. Trans. Roy. Soc. B*, **2011**, 366, 3572-3583.
[14]. C Gérard; A Goldbeter, *Interface Focus*, **2011**, 1, 24-35.
[15]. WY Fu; K Cheng; AKY Fu; NY Ip, *Neurosci.*, **2011**, 180, 353-359.

[16].C-Y Ou; VY Poon; CI Maeder; S Watanabe; EK Lehrman, et al., *Cell*, **2010**, 141, 846-858.
[17].A Errico; K Deshmukh; Y Tanaka; A Pozniakovsky; T Hunt, *Adv. Enz. Regul.*, **2010**, 50, 375-399.
[18].A Echalier; JA Endicott; MEM Noble, *BBA Prto. Proteon.*, **2010**, 1804, 511-519.
[19].B Jia; E Choy; G Cote; D Harmon; S Ye, et al., *Can. Lett.*, **2014**, 342, 104-112.
[20].JA Ducie; P Jelinic; Z Zhang; F Dao; M Bisogna, et al., *Gynecol. Oncol.*, **2014**, 133, Supplement 1, 78.
[21].TJ Chen; YY Lee; CF Li, *Eur. J. Can.*, **2014**, 50, Supplement 4, e68.
[22].C Bruyère; L Meijer, *Curr. Op. Cell Biol.*, **2013**, 25, 772-779.
[23].A Baker; I Verbrugge; K Stanley; J Shortt; R Johnstone, *Exp. Hematol.*, **2013**, 41, S53.
[24].C Xing; H Xie; L Zhou; W Zhou; W Zhang, et al., *Biochem. Biophys. Res. Comm.*, **2012**, 420, 29-35.
[25].M-W Lai; T-C Chen; S-T Pang; C-T Yeh, *Urol. Oncol.: Sem. Orig. Invest.*, **2012**, 30, 871-878.
[26].S Caporali; E Alvino; L Levati; AI Esposito; M Ciomei, et al., *Biochem. Pharmacol.*, **2012**, 84, 598-611.
[27].VM Yenugonda; TB Deb; SC Grindrod; S Dakshanamurthy; Y Yang, et al., *Bioorg. Med. Chem.*, **2011**, 19, 2714-2725.
[28].X Wang; C Sistrunk; ML Rodriguez-Puebla, *Amer. J. Pathol.*, **2011**, 178, 345-354.
[29].SM Manohar; MJ Rathos; V Sonawane; SV Rao; KS Joshi, *Leuk. Res.*, **2011**, 35, 821-830.
[30].MR Hasan; IT Tai, *Gastroenterol.*, **2011**, 140, S-823.
[31].D Askew; T Pareek; S Eid; M Keller; R Guardia-Wolff, et al., *Biol. Blood Marrow Transpl.*, **2011**, 17, S160.
[32].T Ishimaru; J Lau; AL Jackson; JF Modiano; RH Weiss, *J. Urol.*, **2010**, 184, 2143-2149.
[33].M Georgitsi, *Best Pract. Res. Clin. Endocrin. Metab.*, **2010**, 24, 425-437.
[34].ES Child; T Hendrychová; K McCague; A Futreal; M Otyepka; DJ Mann, *BBA Mol. Cell. Res.*, **2010**, 1803, 858-864.
[35].S Wang; PM Fischer, *Trends Pharmacol Sci.*, **2008**, 29, 302-313.
[36].A Putey; G Fournet; O Lozach; L Perrin; L Meijer; B Joseph, *Eur. J. Med. Chem.*, **2014**, 83, 617-629.
[37].G Németh; Z Greff; A Sipos; Z Varga; R Székely, et al., *J. Med. Chem.*, **2014**, 57, 3939-3965.
[38].M Zatloukal; R Jorda; T Gucký; E Řezníčková; J Voller, et al., *Eur. J. Med. Chem.*, **2013**, 61, 61-72.
[39].H Shao; S Shi; S Huang; AJ Hole; AY Abbas, et al., *J. Med. Chem.*, **2013**, 56, 640-659.
[40].H Shao; S Shi; DW Foley; F Lam; AY Abbas, et al., *Eur. J. Med. Chem.*, **2013**, 70, 447-455.
[41].E Schonbrunn; S Betzi; R Alam; MP Martin; A Becker, et al., *J. Med. Chem.*, **2013**, 56, 3768-3782.
[42].J N'Gompaza-Diarra; K Bettayeb; N Gresh; L Meijer; N Oumata, *Eur. J. Med. Chem.*, **2012**, 56, 210-216.
[43].J Malmström; J Viklund; C Slivo; A Costa; M Maudet, et al., *Bioorg. Med. Chem. Lett.*, **2012**, 22, 5919-5923.
[44].AJ Hole; S Baumli; H Shao; S Shi; S Huang, et al., *J. Med. Chem.*, **2012**, 56, 660-670.
[45].AD William; ACH Lee; KC Goh; S Blanchard; A Poulsen, et al., *J. Med. Chem.*, **2011**, 55, 169-196.
[46].R Jorda; L Havlíček; IW McNae; MD Walkinshaw; Ji Voller, et al., *J. Med. Chem.*, **2011**, 54, 2980-2993.
[47].M Toumi; M Barbazanges; SHB Kroll; H Patel; S Ali, et al., *Tetrahed. Lett.*, **2010**, 51, 6126-6128.
[48].K Paruch; MP Dwyer; C Alvarez; C Brown; T-Y Chan, et al., *ACS Med. Chem. Lett.*, **2010**, 1, 204-208.
[49].P Lan; W-N Chen; G-K Xiao; P-H Sun; W-M Chen, *Bioorg. Med. Chem. Lett.*, **2010**, 20, 6764-6772.
[50].DA Heathcote; H Patel; SHB Kroll; P Hazel; M Periyasamy, et al., *J. Med. Chem.*, **2010**, 53, 8508-8522.
[51].D Caridha; AK Kathcart; D Jirage; NC Waters, *Bioorg. Med. Chem. Lett.*, **2010**, 20, 3863-3867.
[52].B Lei; L Xi; J Li; H Liu; X Yao, *Anal. Chim. Acta*, **2009**, 644, 17-24.
[53].CJ Helal; Z Kang; JC Lucas; T Gant; MK Ahlijanian, et al., *Bioorg. Med. Chem. Lett.*, **2009**, 19, 5703-5707.
[54].KL Stevens; MJ Reno; JB Alberti; DJ Price; LS Kane-Carson, et al., *Bioorg. Med. Chem. Lett.*, **2008**, 18, 5758-5762.
[55].J Lee; H Choi; K-H Kim; S Jeong; J-W Park, et al., *Bioorg. Med. Chem. Lett.*, **2008**, 18, 2292-2295.
[56].CD Jones; DM Andrews; AJ Barker; K Blades; KF Byth, et al., *Bioorg. Med. Chem. Lett.*, **2008**, 18, 6486-6489.
[57].H Galons; L Meijer; N Oumata; K Bettayeb, *Biomed. Pharmacother.*, **2008**, 62, 429.
[58].MRV Finlay; DG Acton; DM Andrews; AJ Barker; M Dennis, et al., *Bioorg. Med. Chem. Lett.*, **2008**, 18, 4442-4446.
[59].M Anderson; DM Andrews; AJ Barker; CA Brassington; J Breed, et al., *Bioorg. Med. Chem. Lett.*, **2008**, 18, 5487-5492.
[60].L Aixiao; B Florent; M François; D Michel; W Baoshan, *J. Mol. Struct. Theochem*, **2008**, 849, 62-75.
[61].DE Walters, *J. Med. Chem.*, **2007**, 50, 4787-4787.
[62].J Li; H Liu; X Yao; M Liu; Z Hu; B Fan, *Anal. Chim. Acta*, **2007**, 581, 333-342.
[63].S Huang; R Lin; Y Yu; Y Lu; PJ Connolly, et al., *Bioorg. Med. Chem. Lett.*, **2007**, 17, 1243-1245.
[64].S Huang; R Li; PJ Connolly; S Emanuel; A Fuentes-Pesquera, et al., *Bioorg. Med. Chem. Lett.*, **2007**, 17, 2179-2183.

[65].N Dessalew; PV Bharatam, *Eur. J. Med. Chem.*, **2007**, 42, 1014-1027.
[66].J Subramanian; S Sharma; C B-Rao, *J. Med. Chem.*, **2006**, 49, 5434-5441.
[67].V Kryštof; P Cankař; I Fryšová; J Slouka; G Kontopidis, et al., *J. Med. Chem.*, **2006**, 49, 6500-6509.
[68].S Huang; R Li; PJ Connolly; S Emanuel; SA Middleton, *Bioorg. Med. Chem. Lett.*, **2006**, 16, 4818-4821.
[69].DS Williamson; MJ Parratt; JF Bower; JD Moore; CM Richardson, et al., *Bioorg. Med. Chem. Lett.*, **2005**, 15, 863-867.
[70].M Noble; P Barrett; J Endicott; L Johnson; J McDonnell, et al., *BBA Prto. Proteon.*, **2005**, 1754, 58-64.
[71].R Lin; Y Lu; SK Wetter; PJ Connolly; IJ Turchi, et al., *Bioorg. Med. Chem. Lett.*, **2005**, 15, 2221-2224.
[72].C Hamdouchi; B Zhong; J Mendoza; E Collins; C Jaramillo, et al., *Bioorg. Med. Chem. Lett.*, **2005**, 15, 1943-1947.
[73].MF Braña; M Cacho; ML García; EP Mayoral; B López, et al., *J. Med. Chem.*, **2005**, 48, 6843-6854.
[74].Y Bathini; I Singh; PJ Harvey; PR Keller; R Singh, et al., *Bioorg. Med. Chem. Lett.*, **2005**, 15, 3881-3885.
[75].EW Yue; SV DiMeo; CA Higley; JA Markwalder; CR Burton, et al., *Bioorg. Med. Chem. Lett.*, **2004**, 14, 343-346.
[76].R Solís-Gutiérrez; JS Gómez-Jeria, *Res. J. Pharmac. Biol. Chem. Sci.*, **2014**, 5, 1401-1416.
[77].F Salgado-Valdés; JS Gómez-Jeria, *J. Quant. Chem.*, **2014**, 2014 Article ID 431432, 1-15.
[78].DI Pino-Ramírez; JS Gómez-Jeria, *Amer. Chem. Sci. J.*, **2014**, 4, 554-575.
[79].D Muñoz-Gacitúa; JS Gómez-Jeria, *J. Comput. Methods Drug Des.*, **2014**, 4, 48-63.
[80].D Muñoz-Gacitúa; JS Gómez-Jeria, *J. Comput. Methods Drug Des.*, **2014**, 4, 33-47.
[81].JS Gómez-Jeria; J Molina-Hidalgo, *J. Comput. Methods Drug Des.*, **2014**, 4, 1-9.
[82].JS Gómez-Jeria, *J. Comput. Methods Drug Des.*, **2014**, 4, 32-44.
[83].JS Gómez-Jeria, *Res. J. Pharmac. Biol. Chem. Sci.*, **2014**, 5, 2124-2142.
[84].JS Gómez-Jeria, *Der Pharma Chem.*, **2014**, 6, 64-77.
[85].JS Gómez-Jeria, *SOP Trans. Phys. Chem.*, **2014**, 1, 10-28.
[86].JS Gómez-Jeria, *Brit. Microbiol. Res. J.*, **2014**, 4, 968-987.
[87].JS Gómez-Jeria, *Der Pharm. Lett.*, **2014**, 6., 95-104.
[88].JS Gómez-Jeria, *Int. Res. J. Pure App. Chem.*, **2014**, 4, 270-291.
[89].I Reyes-Díaz; JS Gómez-Jeria, *J. Comput. Methods Drug Des.*, **2013**, 3, 11-21.
[90].A Paz de la Vega; DA Alarcón; JS Gómez-Jeria, *J. Chil. Chem. Soc.*, **2013**, 58, 1842-1851.
[91].JS Gómez-Jeria; M Flores-Catalán, *Canad. Chem. Trans.*, **2013**, 1, 215-237.
[92].T Bruna-Larenas; JS Gómez-Jeria, *Int. J. Med. Chem.*, **2012**, 2012 Article ID 682495, 1-16.
[93].C Barahona-Urbina; S Nuñez-Gonzalez; JS Gómez-Jeria, *J. Chil. Chem. Soc.*, **2012**, 57, 1497-1503.
[94].JS Gómez-Jeria, *J. Chil. Chem. Soc.*, **2010**, 55, 381-384.
[95].JS Gómez-Jeria; F Soto-Morales; J Rivas; A Sotomayor, *J. Chil. Chem. Soc.*, **2008**, 53, 1393-1399.
[96].JS Gómez-Jeria; F Soto-Morales; G Larenas-Gutierrez, *Ir. Int. J. Sci.*, **2003**, 4, 151-164.
[97].JS Gómez-Jeria; L Lagos-Arancibia; E Sobarzo-Sánchez, *Bol. Soc. Chil. Quím.*, **2003**, 48, 61-66.
[98].JS Gómez-Jeria; M Ojeda-Vergara, *Int. J. Quant. Chem.*, **1997**, 61, 997-1002.
[99].JS Gómez-Jeria; M Ojeda-Vergara; C Donoso-Espinoza, *Mol. Engn.*, **1995**, 5, 391-401.
[100]. JS Gómez-Jeria; P Sotomayor, *J. Mol. Struct. (Theochem)*, **1988**, 166, 493-498.
[101]. JS Gómez-Jeria; D Morales-Lagos; JI Rodriguez-Gatica; JC Saavedra-Aguilar, *Int. J. Quant. Chem.*, **1985**, 28, 421-428.
[102]. JS Gómez-Jeria; DR Morales-Lagos, *J. Pharm. Sci.*, **1984**, 73, 1725-1728.
[103]. JS Gómez-Jeria; D Morales-Lagos, "The mode of binding of phenylalkylamines to the Serotonergic Receptor," in *QSAR in design of Bioactive Drugs*, M. Kuchar Ed., pp. 145-173, Prous, J.R., Barcelona, Spain, 1984.
[104]. K Fukui; H Fujimoto, *Frontier orbitals and reaction paths: selected papers of Kenichi Fukui*, World Scientific, Singapore; River Edge, N.J., 1997.
[105]. JS Gómez-Jeria, *Canad. Chem. Trans.*, **2013**, 1, 25-55.
[106]. JS Gómez-Jeria, *Elements of Molecular Electronic Pharmacology (in Spanish)*, Ediciones Sokar, Santiago de Chile, 2013.
[107]. MJ Frisch; GW Trucks; HB Schlegel; GE Scuseria; MA Robb, et al., Gaussian98 Rev. A.11.3, Gaussian, Pittsburgh, PA, USA, 2002.
[108]. JS Gómez-Jeria, D-Cent-QSAR: A program to generate Local Atomic Reactivity Indices from Gaussian log files. 1.0, Santiago, Chile, 2014.
[109]. JS Gómez-Jeria, *J. Chil. Chem. Soc.*, **2009**, 54, 482-485.
[110]. JS Gómez-Jeria; M Ojeda-Vergara, *J. Chil. Chem. Soc.*, **2003**, 48, 119-124.
[111]. Statsoft, Statistica 8.0, 2300 East 14 th St. Tulsa, OK 74104, USA, 1984-2007.

[112]. U Varetto, Molekel 5.4.0.8, Swiss National Supercomputing Centre: Lugano, Switzerland, 2008.
[113]. RD Dennington; TA Keith; JM Millam, GaussViev 5.0.8, 340 Quinnipiac St., Bldg. 40, Wallingford, CT 06492, USA, 2000-2008.
[114]. Chemaxon, MarvinView, www.chemaxon.com, USA, 2014.
[115]. Hypercube, Hyperchem 7.01, 419 Phillip St., Waterloo, Ontario, Canada, 2002.